SCIENTIFIC REPORTS

OPEN

SUBJECT AREAS:
ELECTRONIC PROPERTIES AND MATERIALS
TOPOLOGICAL INSULATORS

Received
2 July 2014

Accepted
30 December 2014

Published
27 January 2015

Correspondence and requests for materials should be addressed to K.L.T. (eleteokl@nus.edu.sg) or W.L. (lan.wang@rmit.edu.au)

Gate-tuned quantum oscillations of topological surface states in β-Ag_2Te

Azat Sulaev[1], Weiguang Zhu[2], Kie Leong Teo[3] & Lan Wang[1,4]

[1]School of Physical and Mathematical Sciences, Division of Physics and Applied Physics, Nanyang Technological University, Singapore 637371, [2]School of Electronics and Electrical Engineering, Nanyang Technological University, Singapore 639789, [3]Department of Electrical and Computer Engineering, National University of Singapore, Singapore 117576, [4]School of Applied Sciences, RMIT University, Melbourne, VIC 3000, Australia.

We report the strong experimental evidence of the existence of topological surface states with large electric field tunability and mobility in β-Ag_2Te. Pronounced 2D Shubnikov-de Haas oscillations have been observed in β-Ag_2Te nanoplates. A Berry phase is determined to be near π using the Landau level fan diagram for a relatively wide nanoplate while the largest electric field ambipolar effect in topological insulator so far (~2500%) is observed in a narrow nanoplate. The π Berry phase and the evolution of quantum oscillations with gate voltage (V_g) in the nanoplates strongly indicate the presence of topological surface states in β-Ag_2Te. Moreover, the mobility of the narrow Ag_2Te nanoplate is about several thousand $cm^2s^{-1}V^{-1}$. Our results suggest that β-Ag_2Te has the potential to become an important material in the investigation of topological insulators.

Topological insulator (TI) is a state of quantum matter characterized by Z_2 invariance[1–4]. It is an insulator in the bulk state but manifests conducting helical states at the boundary. The exotic boundary states of TIs are expected to form a playground of various topological quantum effects and show great potential in spintronics and quantum computation. Since the first experimental realization of TI in CdTe/HgTe/CdTe quantum well structures[5], an extensive effort has been put up in search for new TI systems. To date, CdTe/HgTe/CdTe[5] and InAs/GaSb[6] have been experimentally confirmed to be two-dimensional TIs while strained HgTe and many Bi based compounds such as Bi_xSb_{1-x}, Bi_2Se_3 and Bi_2Te_3 have been realized as three-dimensional TIs[7–26]. To explore the possible application of TI in spintronics, ideal TI systems are expected to exhibit high mobility and gate electric field tunability. However, most of the TI materials show very small surface contribution due to defect-induced large bulk contribution and therefore electric field tunability cannot be realized. On the other hand, very few TIs that manifest electric field ambipolar effect such as $Bi_{2-x}Sb_xTe_{3-y}Se_y$[27–29] and thin Bi_2Se_3 flakes[21,25], show low mobility. On this basis, it is important to identify new TIs that show large gate electric field tunability and high surface mobility for the application of future TI based spintronic devices.

The β-Ag_2Te is known for its unusual large and non-saturating quasi-linear magnetoresistance (MR) in the field range of 10–10^5 Oe and temperature range of 5–300 K[30–32]. The origin of this unusual property has generated much debate since its discovery and may be associated with its 3D-TI nature. Theoretical calculation suggests that β-Ag_2Te is a TI with anisotropy and the unusual MR is largely originated from electrical transport on the topological surface states[33]. Recently, Aharonov-Bohm (AB) oscillations have been observed in a nanowire of β-Ag_2Te which indicates the existence of surface states[34,35]. However, the topological nature of the surface state still remains to be confirmed.

In this paper, we report further experimental evidence of the existence of topological surface states in β-Ag_2Te. Especially, the topological surface state of narrow Ag_2Te nanoplate exhibits the largest electric field ambipolar effect in TI so far (~2500%). We fabricated nanoplate devices as shown in the inset of Fig. 1(a) and Fig. 1(b). Both devices show pronounced two dimensional (2D) SdH oscillations. Using the measured resistivity ρ_{xx} and Hall resistivity ρ_{xy} of the wide nanoplate as shown in Fig. 1(a), the conductivity σ_{xx} is calculated and the Berry phase is determined to be near π by Landau Level (LL) fan diagram. This reveals that the SdH oscillation originates from the topological surface states. Utilizing the large ambipolar field effect of the narrow nanoplate as shown in Fig. 1(b), the evolution of SdH oscillations with applied gate voltage (V_g) was investigated and also strongly indicates a Dirac cone composed surface state. Moreover, the mobility of the surface transport of the narrow β-Ag_2Te nanoplate is determined to be several thousand $cm^2s^{-1}V^{-1}$. Finally, the MR variation with V_g of the narrow nanoplate indicates a correlation effect between the bulk electrons and Dirac fermions.

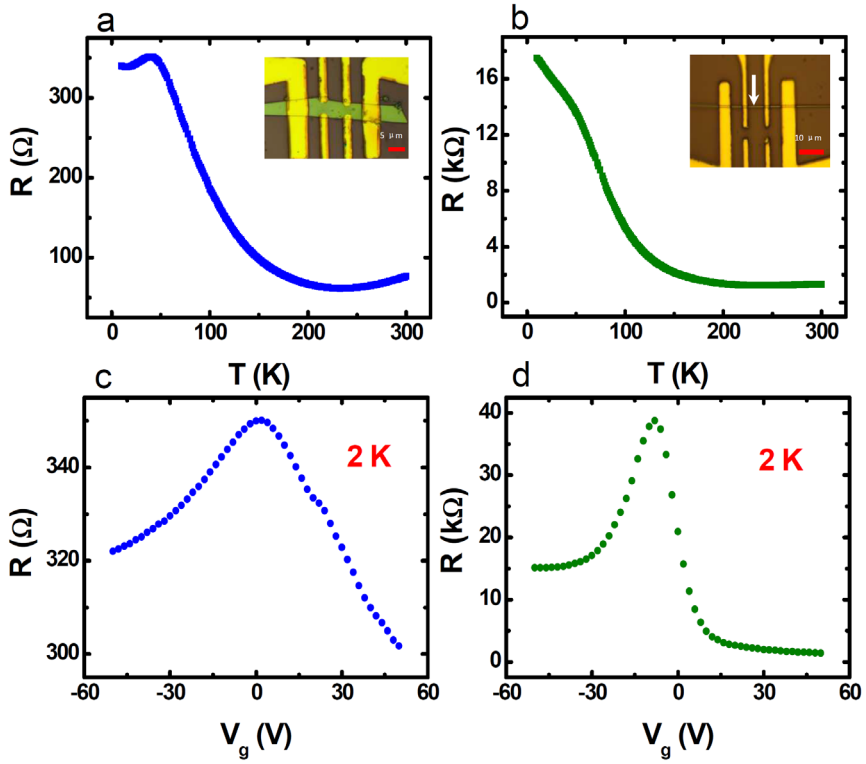

Figure 1 | Temperature and voltage dependence of resistance. (a) and (b) show the temperature dependence of resistance of β-Ag_2Te wide and narrow nanoplates, respectively. The insets show the corresponding device images. The red bars are 5 μm and 10 μm in (a) and (b), respectively. The arrow in (b) points to the narrow nanoplates. (c) and (d) show the V_g dependence of resistance of β-Ag_2Te at 2 K.

Results

Temperature and gate voltage dependence of resistance. The typical transport behavior of two devices fabricated from a relatively wide nanoplate and a narrow nanoplate grown by CVD methods are shown in Fig. 1(a)–(d). It should be emphasized that similar results have been repeated in several devices fabricated using wide and narrow nanoplates. The wide β-Ag_2Te nanoplates tend to be slightly n-type. The inset of Fig. 1(a) and Fig. 1(b) show the fabricated devices using heavily p-doped Si with 300 nm thick of SiO_2 dielectric layer. The thicknesses and widths for the two nanoplate devices are 120 nm (thickness), 5 μm (width) and 98 nm (thickness), 395 nm (width), respectively. As shown in Fig. 1(a), the resistance (R_{xx}) of the relatively wide nanoplate decreases slightly with temperature from T = 300 K to 250 K, then increases about several times from 250 K to 30 K, and finally decreases to 10 K. The special temperature dependence of R_{xx} of the nanoplate is due to the light impurity doping, which has been observed in many doped semiconductor systems[36]. The metallic behavior at low temperature of the nanoplate is attributed to the conduction in the impurity band, while the metallic behavior when $T > 250$ K can be explained by the thermal excitation of electrons from the Anderson localized states to extended states above the mobility edge. A better stoichiometry is achieved in the narrow nanoplate, and hence we observed much sharper increase of resistance with decreasing temperature as shown in Fig. 1(b). The gradually saturating behavior at low temperatures is due to the surface states. To probe the existence of surface states, we have performed the gate-tuned resistance measurement. As shown in Fig. 1(c), the R_{xx} of the wide nanoplate only changes slightly with V_g in view of electron doping. Although the V_g dependence of R_{xx} shows a peak near 0 V, the voltage dependence of Hall resistance (R_{xy}) and SdH oscillations indicates that electric field ambipolar gate effect cannot be realized in wide nanoplate devices due to charge doping. The resistance change with an applied gate voltage may originate from the variation of the density of states at the Fermi level in the bulk states when the Fermi level is slightly shifted by the gate electric field. We observed the phenomenon in several wide nanoplate samples. In contrast to wide nanoplates, the narrow nanoplates shows a huge ambipolar type electric field effect under a back V_g, which further confirms the high stoichiometry as indicated by the temperature dependence of resistivity curve. Fig. 1(d) shows that the gate induced resistance change ($R_{peak}/R_{+50\ V}$) in the narrow β-Ag_2Te nanoplate is ~2500%, a value which is much larger than that obtained in any other TIs. Here, the R_{peak} and $R_{+50\ V}$ is the resistance at the peak of the ambipolar curve and V_g = +50 V, respectively. The sharp transition at highest resistance point (the charge neutrality point) and the gradual change of resistance when the V_g deviates from the charge neutrality point indicate that the ambipolar behavior could be due to topological surface states of Dirac cone. However, it should be emphasized that the ambipolar electric field effect can also be realized in semimetal or semiconductor with a very narrow band gap. In order to probe the topological nature of the surface state, we have performed two experiments. We first determine the Berry phase from the SdH oscillation of the conductivity of the wide nanoplate and then investigate the evolution of SdH oscillation with V_g since the narrow nanoplate shows huge V_g dependence of resistance of Dirac cone type.

Berry phase obtained from SdH oscillations. Figure 2(a) shows the R_{xy} of the wide nanoplate device under tilted magnetic field (B) as a function of the component of the magnetic field perpendicular to the sample surface ($B_\perp$). The angle (θ) is defined between the B field and sample surface. The R_{xy} indicates an n-type carrier and a clear deviation from the linear relationship with B field. This demonstrates that there are more than one transport channel with different mobility values. At higher field, the R_{xy} oscillates periodically in 1/B, which is the standard behavior of SdH oscillation. More importantly, we observe that the positions of maxima and minima do not change

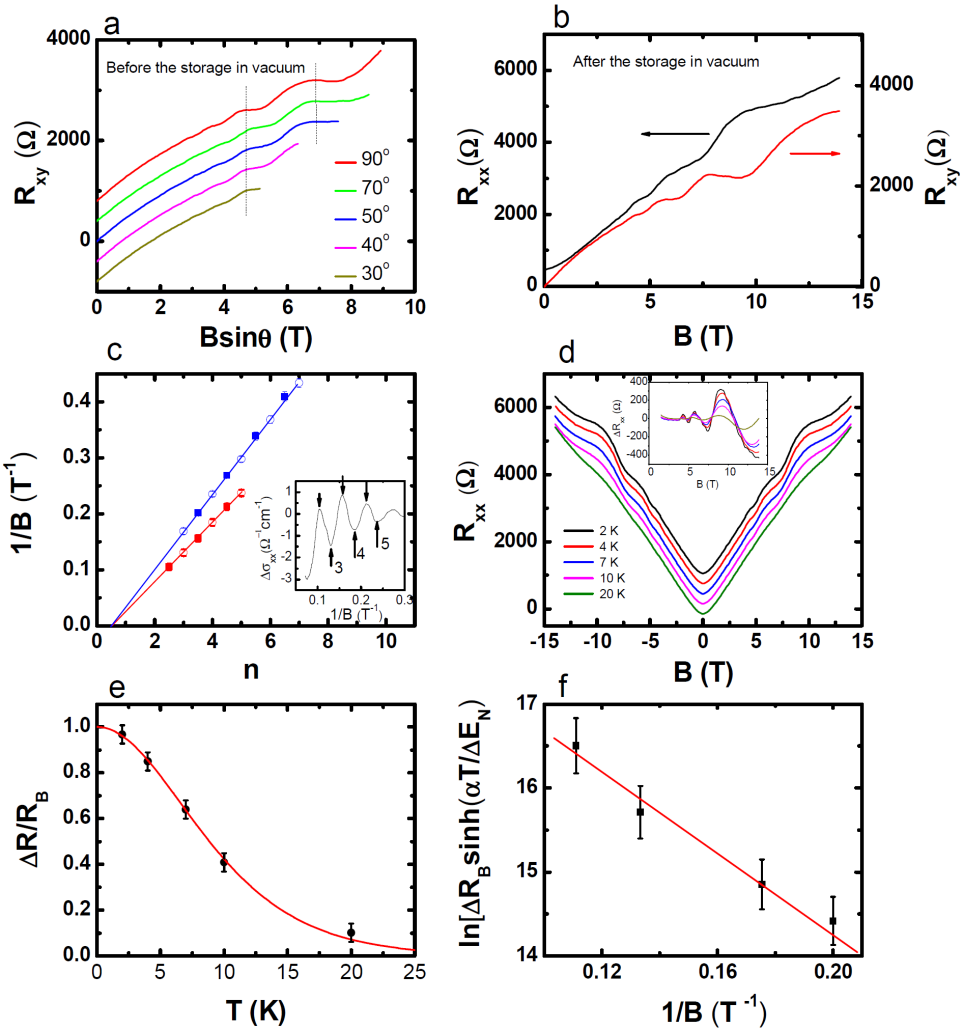

Figure 2 | SdH oscillations and fan diagram analysis. (a) Hall resistance (R_{xy}) as a function of the *B* field measured at various tilted angles (θ); (b) R_{xx} and R_{xy} as functions of the *B* field with θ = 90°. The measurements were performed using the same sample for (a), which had been stored for three days in vacuum after the measurements in (a); (c), SdH fan diagrams for measured 1/B with the filling factor n. The blue and red data and fitting lines are for the device before the storage and after the storage, respectively. The squares and circles are the maxima and minima, respectively. The inset shows the $\Delta\sigma_{xx}$ vs. 1/B plot for the device after the storage; (d) R_{xx} vs. *B* field curves at various temperatures. The inset shows the SdH oscillation after subtracting the background MR. (e) The temperature dependence of relative amplitude of SdH oscillation in $\Delta R_{xx}(B)$ for the 3rd LL. The solid line is a fit to $\frac{\alpha T/\Delta E_N(B)}{\sinh[\alpha T/\Delta E_N(B)]}$; (f) $\ln(\Delta RB\sinh(\alpha T/\Delta E_N))$ is plotted as a function of 1/B.

with $B_\perp$ field. This clearly indicates that the oscillations originate from 2D transport behavior. No oscillations are observed in R_{xx} vs B curve (not shown here) when the applied magnetic field is parallel to the sample surface, which further supports the 2D transport and rules out the oscillation from bulk in this sample. The lack of the SdH oscillations from bulk electrons indicates low mobility of the bulk transport in this device.

A prominent property of Dirac fermions is that they carry the Berry phase of π. The observation of a π phase shift in SdH oscillation would clearly demonstrate that the 2D transport is indeed due to the topological surface transport[4,37]. SdH oscillations originate from successive emptying of Landau Levels (LL) with increasing magnetic field. The LL index n is related to the cross section area S_F of the Fermi surface by

$$2\pi(n+\gamma) = S_F\frac{\hbar}{eB} \qquad (1)$$

where $\gamma = 0$ or 1/2 for topological trivial electrons and Dirac Fermions, respectively, *e* is the electron charge, h is the Planck constant ($\hbar = \frac{h}{2\pi}$), and B is the magnetic flux density. Fig. 2(b) is the R_{xy} and R_{xx} of the wide nanoplate with a storage in vacuum for three days after the measurement in Fig. 2(a). As shown in Fig. 2(b), the SdH oscillation of R_{xy} changes after the storage in vacuum, which indicates the doping of surface or bulk states. To obtain the value of Berry phase of the system, we calculate the conductivity using the formula $\sigma_{xx} = \rho_{xx}/(\rho_{xx}^2 + \rho_{xy}^2)$ for both measurements in Fig. 2(a) and Fig. 2(b). Thereafter the $\Delta\sigma_{xx}$ is obtained through a smooth back ground subtraction. The $\Delta\sigma_{xx}$ vs 1/B curves for both conditions show oscillations of a single period which indicates only one transport channel in the surface states of the sample contributing to the oscillations. The inset of Fig. 2(c) is the $\Delta\sigma_{xx}$ vs 1/B curve obtained from Fig. 2(b). The LL fan diagrams based on the oscillations of the conductivity for both situation are shown in Fig. 2(c), where their minima are identified to signify the integer n (indicated by arrows), while the half integers n + 1/2 are assigned to the positions of maxima (indicated by arrows). The interception at 1/B = 0 should be at n = 0 (for the topological trivial surface states) or n = 1/2 (for the topological surface states). As shown in Fig. 2(c), linear fits to the data give interception of 0.52 (the blue fitting line) and 0.54 (the red fitting line) for the sample before the storage and after the storage, respectively. The values are close to the

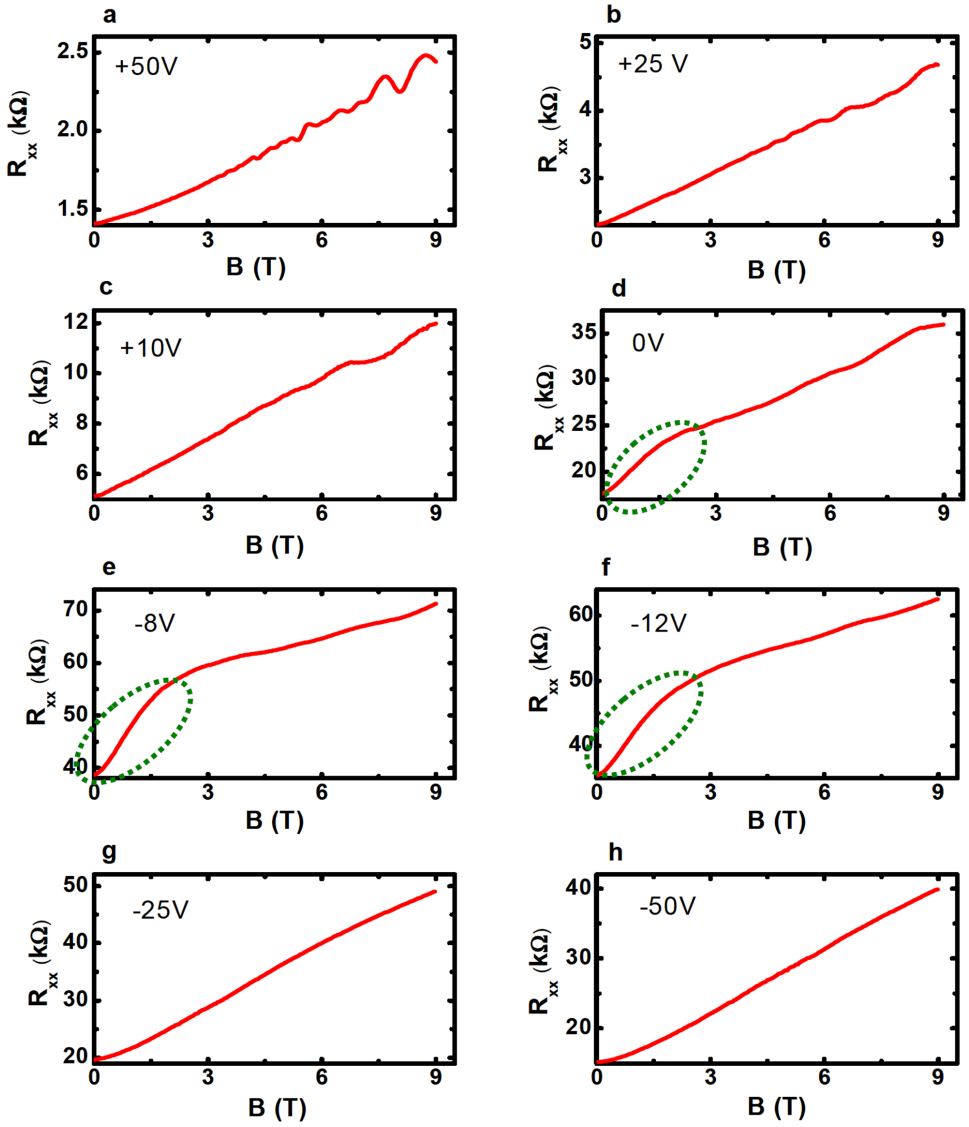

Figure 3 | R_{xx} of the narrow plate as a function of *B* field measured under various V_g. (a) +50 V, (b) +25 V, (c) +10 V, (d) 0 V, (e) −8 V, (f) −12 V, (g) −25 V and (h) −50 V.

value of 0.5 expected for Dirac fermions. This result strongly supports that the SdH oscillation is indeed originated from the topological surface states. The doping due to the storage can shifts the Fermi level, but it does not change the topological characteristics.

Figure 2(d) displays the temperature dependence of SdH oscillations of R_{xx}. The inset shows the ΔR_{xx} obtained from R_{xx} by subtracting a polynomial fit to the background. The amplitude of the SdH oscillations decreases with increasing temperature due to thermal agitation of electrons on the Landau levels. We have used the standard Lifshitz-Kosevich theory

$$\Delta R_{xx}(T,B) \propto \frac{\alpha T/\Delta E_N(B)}{\sinh[\alpha T/\Delta E_N(B)]} e^{-\alpha T_D/\Delta E_N(B)} \qquad (2)$$

to fit the temperature dependence of SdH oscillations, where $\Delta E_N = heB/2\pi m^* c$ is the energy gap between Nth and (N + 1)th Landau Level, $T_D = h/4\pi^2\tau k_B$ is the Dingle temperature, and $\alpha = 2\pi^2 k_B$. The B, h, m^*, k_B, and c are the magnetic field, Planck constant, the effective mass of carriers, Boltzmann constant, and speed of light, respectively. The temperature dependence of $\Delta R/\Delta R(0\ K)$ for the 3rd Landau level is plotted in Fig. 2(e). The solid line is a fit to $\frac{\alpha T/\Delta E_N(B)}{\sinh[\alpha T/\Delta E_N(B)]}$. The ΔR (0 K) is the ΔR at 0 K obtained from the fitting and m^* can be calculated using the fitted value of E_N. We averaged the value obtained for different B to get $m^* = 0.12\ m_e$. From the slope of the semi-log plot of $\Delta RB \sinh(\alpha T/\Delta E_N)$ vs $1/B$ at $T = 2$ K, the T_D is determined to be 13.6 K and the carrier life-time is calculated to be 8.9×10^{-14} s. The mobility is then determined to be 1310 $cm^2 s^{-1} V^{-1}$.

SdH oscillations with gate. The existence of Dirac cone composed topological surface states can be further investigated by examining the evolution of the SdH oscillation in the narrow nanoplate through back gating. From Eq. (1), we know that the period of R_{xx} vs 1/B is determined by the cross section of Fermi surface as shown in Eq. (3),

$$\Delta\frac{1}{B} = \frac{2\pi e}{\hbar S_F} \qquad (3)$$

Assuming a circular 2D Fermi surface or a spherical 3D Fermi surface, the value of Fermi wave vector k_F can be calculated using $S_F = \pi k_F^2$. Thereafter, the carrier density of 2D surface states and 3D bulk states can be calculated by $n_{2D} = \frac{k_F^2}{2\pi}$ and $n_{3D} = \frac{k_F^3}{3\pi^2}$, respectively.

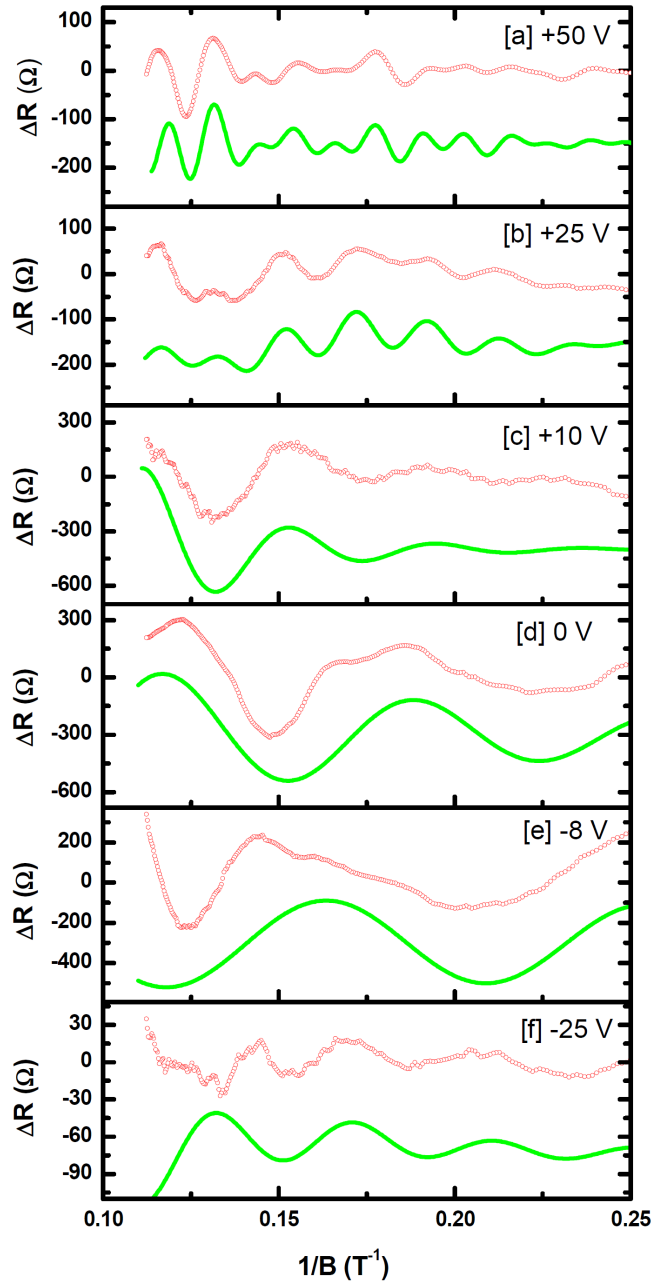

Figure 4 | ΔR_{xx} as a function of 1/B field with various Vg. (a) +50 V, (b) +25 V, (c) +10 V, (d) 0 V, (e) −8 V, (f) −25 V. The red circles are the experimental data. The green lines are the fitting curves.

The dependence of R_{xx} on *B* field under various V_g was performed and the results are shown in Fig. 3(a)–(h). To analyze the SdH oscillations, ΔR_{xx} is obtained from R_{xx} by subtracting a polynomial fit to the background. The ΔR_{xx} vs 1/B curves with various V_gs are shown in Fig. 4(a)–(f). The curves at −12 V and −50 V do not show reasonable SdH oscillations, which may contribute to the very small Fermi surface and large noise, respectively. From Fig. 4, it is clearly evident that the period of SdH oscillation rises when V_g varies from +50 V to −8 V. This demonstrates that the area of Fermi surface decreases when V_g changes from +50 V to −8 V. With further increasing amplitude of V_g to the negative direction, the magnitude of SdH oscillations gradually diminishes. The SdH oscillations can still be clearly observed and the period of the oscillations decreases when V_g varies from −8 V to −25 V. This demonstrates that the area of Fermi surface increases in the procedure. This correlates well with the scenario that the area of the Fermi surface increases with the Fermi level shifting away from the Dirac point. In order to understand the band structure of β-Ag_2Te, we fit the ΔR_{xx} vs 1/B curve with the theoretical expression for SdH oscillations. The formula can be written as

$$\Delta R_{xx} = A\exp(-\pi/\mu B)\cos[2\pi(B_F/B + 1/2 + \beta)] \quad (4)$$

where B_F is the frequency of the SdH oscillation, A is the amplitude, μ is the mobility of carriers, and β is the Berry phase[22,23]. Equation (4) is in fact a zero temperature formula, which considers the effect of finite relaxation time but ignores the temperature effect[38]. As the accurate phase analysis should use the value of conductivity $\sigma_{xx} = \rho_{xx}/(\rho_{xx}^2 + \rho_{xy}^2)$, especially for systems like β-Ag_2Te that has similar values of ρ_{xx} and ρ_{xy}, the β value obtained in the fitting to ΔR_{xx} cannot provide the information of topological nature[4]. Here, we focus on two fitting parameters, the B_F and μ. The experimental data (red circles) and fitting curves (green lines) are shown in Fig. 4. In the fitting process, the B_F values are first roughly determined by inspection and FFT transformation. Thereafter, accurate B_Fs and μs are fitted. Three transport channels are employed to fit the SdH oscillations at V_g = +50 V and V_g = +25 V. One transport channel is utilized to fit the oscillations at other applied V_gs. The SdH oscillations at −8 V (Fig. 4(e)) show an abrupt increase at the large field, which probably originates from the deviation of background subtraction. A large deviation at large field can appear when the number of oscillations is small. The phase deviation of the fitting at large field (1/B < 0.15 T^{-1} or B > 6.7 T) at −25 V (Fig. 4(f)) may result from the large noise of the data and error in background subtraction. The three peaks and three valleys in low field range of 0.15 T^{-1} < 1/B < 0.25 T^{-1} clearly indicates a larger oscillation period compared with that at V_g = 0 V and −8 V. Although the fittings deviate in some features, our fitting do reveal the main features of the experimental data. The fitted B_Fs and μs are shown in table 1. Based on the B_F values, the values of k_Fs are calculated as listed in the table. The V_g dependence of k_F is depicted in Fig. 5(a), in which both the negative and positive value of k_F is plotted as the red squares. For the SdH at +50 V and +25 V, we choose the largest B_F to calculate the k_F. The green dashed line is drawn to clearly depict the cone structure. As previously discussed, the ambipolar effect can originate from the topological surface or bulk state of a semimetal. For the same Fermi surface area perpendicular to *B* field, the bulk state has a much larger carrier density. Using the formulae as aforementioned, the calculated carrier densities at +50 V are $n_{3D} = 4.3 \times 10^{18}$ cm^{-3} for the bulk state of semimetal and $n_{2D} = 4.0 \times 10^{12}$ cm^{-2} for the Dirac cone composed surface state. At 0 V, the corresponding values for n_{3D} and n_{2D} are 3.0×10^{17} cm^{-3} and 6.8×10^{11} cm^{-2}, respectively. We note that the charge tunability of a 300 nm SiO_2 dielectric layer is about 3.6×10^{12} cm^{-2}/50 V. Considering the sample thickness of 98 nm, if the ambipolar behavior was due to the bulk state, the tuned charge would be 4.2×10^{13} cm^{-2} which is 11 times larger than the tuning ability of a SiO_2 dielectric layer. Thus, our results clearly rule out the possibility of bulk originated ambipolar behavior and provide further strong evidence of the existence of surface states of Dirac cone type. As for the other two channels showing SdH oscillations at V_g = +50 V and +25 V, we speculate that they originate from the Rashba splitting induced topological trivial surface states, which have shown by the Altshuler-Aronov-Spivak oscillations in the β-Ag_2Te nanowire[34].

The V_g dependence of the mobility is shown in Fig. 5(b), the carrier mobility is in the range between ~1×10^3 to ~2×10^3 $cm^2s^{-1}V^{-1}$ when the gate voltage varies from +50 V to +10 V. It increases to ~4×10^3 $cm^2s^{-1}V^{-1}$ at V_g = 0 V and then the mobility decreases to ~2×10^3 $cm^2s^{-1}V^{-1}$ at V_g = −25 V. The obtained mobility values are decent compared with that in other topological insulators[11,19–21,39,40]. It also agrees with the mobility value (1310 $cm^2s^{-1}V^{-1}$) obtained for the doped β-Ag_2Te nanoplate. The shape of the oscillations at −8 V is different from that of the standard SdH oscillation, which indicates a large artefact from subtraction.

Table 1 | The fitting parameter B_F and μ for SdH oscillations, and the calculated k_F from the fitted B_F at various V_gs

	B_F (T)	μ ($\times 10^3$ $cm^2s^{-1}V^{-1}$)	k_F ($\times 10^{-2}$ $Å^{-1}$)
+50 V	83.5 ± 0.5	2.1 ± 0.2	5.04 ± 0.02
	70.5 ± 0.5	1.5 ± 0.2	4.63 ± 0.02
	45.6 ± 0.5	1.4 ± 0.2	3.72 ± 0.02
+25 V	52 ± 0.5	2 ± 0.2	3.98 ± 0.02
	44.1 ± 0.5	2 ± 0.2	3.67 ± 0.02
	10.6 ± 0.5	2.5 ± 0.2	1.80 ± 0.02
+10 V	24 ± 2	1 ± 0.2	2.70 ± 0.1
0 V	14.1 ± 2	4 ± 0.5	2.07 ± 0.2
−8 V	10.2 ± 2.5	30 ± 5	1.75 ± 0.4
−25 V	25.1 ± 1	2 ± 0.3	2.76 ± 0.06

Because the fitted value of μ is closely related to the shape of the SdH oscillation (the decay of the oscillation amplitude), the very large mobility value (3×10^4 $cm^2s^{-1}V^{-1}$ as shown in table 1) at $V_g = -8$ V is probably not reliable. Using the width of the narrow nanoplate (395 nm) and the interval between the contact (7.2 μm), we can calculate the sheet resistance and then calculate the mobility using $\mu = \sigma/en$. Considering the devices have top and bottom surfaces, the calculated mobility at $V_g = 0$ is $\sim 5 \times 10^3$ $cm^2s^{-1}V^{-1}$, which also agrees well with the result obtained from SdH oscillation. For V_gs very near the charge neutrality point, we cannot get accurate k_F due to the lacking of enough oscillations. The variation of MR with V_g in the low field regime also shows an interesting feature. As depicted in Fig. 3(d), (e), (f), the MR presents a relatively sharp increase in the low field regime (circled by green dash lines) at $V_g = 0$ V, −8 V and −12 V, near the charge neutrality point and does not appear in the MR curves under other applied V_g. This may suggest that the π Berry phase induced weak anti-localization can be manifested when the E_F is far away from the bulk band. In all, it is strongly indicated that β-Ag_2Te is a TI from the Berry phase of π obtained from LL fan diagram as shown in Fig. 2(c) and Dirac cone type evolution of SdH oscillations under V_g as depicted in Fig. 3, 4, 5.

The voltage dependence of MR. As aforementioned, the origin of the unusual MR of β-Ag_2Te is still under debate, which may originate from the bulk effect or surface effect[28–32]. To distinguish the bulk from the surface effect, high quality samples with tunable Fermi level are indispensable. It has not been realized prior to this work. Figure 6 shows the comparison of ambipolar effect and MR under applied V_g. The MR is defined as $(R(9T) - R(0T))/R(0T)$, which depicts a clear correlation with the E_F position. The MR displays a lowest value of 78% at V_g of the charge neutrality point. When the V_g deviates from the charge neutrality point, the MR gradually increases in both negative and positive directions and reaches a maximum value at the voltages when the electric field ambipolar effect saturates. Thereafter, the resistance decreases with increasing V_g magnitude in both negative and positive directions. Based on the relationship between the E_F position and electric field ambipolar curve, we can clearly describe the MR behavior in β-Ag_2Te. At the charge neutrality point, the E_F is located at the Dirac point and MR presents the lowest value. When the E_F in the bulk band gap (but on the Dirac type surface states) is moved to the conduction band or valence band, the MR increases continuously until the E_F touches the bulk band. Thereafter, any further manipulation to the bulk causes MR to decrease. Other than the bulk or surface origin of large quasi-linear MR, our experiment provides the possibility of controlling the interplay of bulk and topological surface state[41]. As shown in Fig. 4, the gated MR demonstrates that the largest MR appears near the top of the valence band and bottom of the conduction band, where the bulk electrons and Dirac Fermions can have a strong correlation. We still do not fully understand the correlation effect between the bulk electrons and Dirac Fermions, which deserves further theoretical and experimental investigations.

Discussion

In conclusion, using LL fan diagram obtained from the oscillation of σ_{xx} and the variation in the period of SdH oscillation with applied V_g, we provide strong evidence of the topological nature of surface states in β-Ag_2Te. The topological surface states of highly stoichiometric narrow β-Ag_2Te nanoplate exhibit the largest ambipolar effect in TI so far (~2500%) and decent mobility (a few thousand $cm^2s^{-1}V^{-1}$). This indicates that β-Ag_2Te has the potential to become an important material for TI investigation. Moreover, the first report of V_g dependence of MR in β-Ag_2Te suggests that the interplay between the bulk electrons and surface Dirac fermions has a large effect on MR for this material.

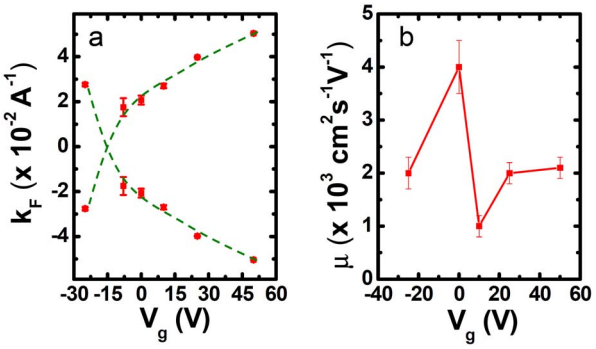

Figure 5 | Vg dependence of k_F and μ. (a) The variation of k_F with V_g. The red squares are the calculated results based on the SdH oscillations. The green lines are plotted to depict the cone structure. (b) The V_g dependence of the carrier mobility μ.

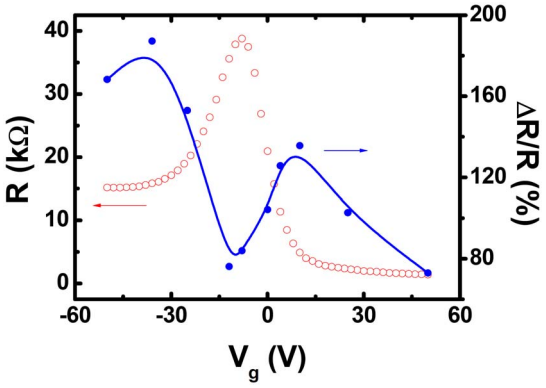

Figure 6 | The MR measured under various applied V_g. The R_{xx} vs V_g curve is plotted for comparison.

Methods

Using standard chemical vapor deposition (CVD) method, we have successfully obtained high quality β-Ag_2Te nanoplates. The details of growth method and characterization can be found in Ref. 31. The thickness of all the nanoplates varies from ~100 nm to ~300 nm, while the width varies from ~100 nm to ~20 μm. It is experimentally observed that the thickness of the β-Ag_2Te nanostructures does not change much with increasing growth time (from 10 mins to 3 hours). Longer growth time only results in the increase of width and length of the nanostructures. Standard photolithography technique was employed to pattern electrodes on the nanoplates. Cr/Au (5 nm/120 nm) contacts were deposited in a magnetron sputtering system with a base pressure of 1×10^{-8} torr. Standard lock-in technique was utilized to perform four-terminal magnetoresistance measurements in two Quantum Design PPMS systems with 9 Tesla and 14 Tesla magnets respectively. All the measurements in this manuscript were carried out from −14 T to 14 T or from −9 T to 9 T, and then the R_{xx} (H) and R_{xy} (H) is calculated using formula

$$R_{xx}(H) = (R_{xx}(+H) + R_{xx}(-H))/2$$
$$R_{xy}(H) = (R_{xy}(+H) - R_{xy}(-H))/2 \quad (5)$$

to eliminate the effect of the non-symmetric contacts.

1. Moore, J. E. The Birth of Topological Insulators. *Nature* **464**, 194–198 (2010).
2. Qi, X. L. & Zhang, S. C. The Quantum Spin Hall Effect and Topological Insulators. *Phys. Today* **63**, 33 (2010).
3. Hasan, M. Z. & Kane, C. L. Topological Insulators. *Rev. Mod.Phys.* **82**, 3045–3067 (2010).
4. Ando, Y. Topological Insulator Materials. *J. Phys. Soc. Jpn.* **82**, 102001 (2013).
5. König, M. *et al.* Quantum Spin Hall Insulator State in HgTe Quantum Wells. *Science* **318**, 766–770 (2007).
6. Knez, I., Du, R. R. & Sullivan, G. Evidence for Helical Edge Modes in Inverted InAs/GaSb Quantum Wells. *Phys. Rev. Lett.* **107**, 136603 (2011).
7. Hancock, J. N. *et al.* Surface State Charge Dynamics of a High – Mobility Three – Dimensional Topological Insulator. *Phys. Rev. Lett.* **107**, 136803 (2011).
8. Checkelsky, J. G., Hor, Y. S., Cava, R. J. & Ong, N. P. Surface State Conduction Observed in Voltage-Tuned Crystals of the Topological Insulator Bi_2Se_3. *Phys. Rev. Lett.* **106**, 196801 (2011).
9. Checkelsky, J. G. *et al.* Quantum Interference in Macroscopic Crystals of Nonmetallic Bi_2Se_3. *Phys. Rev. Lett.* **103**, 246601 (2009).
10. Butch, N. P. *et al.* Strong Surface Scattering in Ultrahigh Mobility Bi_2Se_3 Topological Insulator Crystals. *Phys. Rev. B* **81**, 241301 (2010).
11. Qu, D. X., Hor, Y. S., Xiong, J., Cava, R. J. & Ong, N. P. Quantum Oscillations and Hall Anomaly of Surface States in the Topological Insulator Bi_2Te_3. *Science* **329**, 821–824 (2010).
12. Peng, H. *et al.* Aharonov-Bohm Interference in Topological Insulator Nanoribbons. *Nat. Mater.* **9**, 225–229 (2010).
13. Chen, J. *et al.* Gate-Voltage Control of Chemical Potential and Weak Antilocalization in Bi2Se3. *Phys. Rev. Lett.* **105**, 176602 (2010).
14. Kim, Y. S. *et al.* Thickness-Dependent Bulk Properties and Weak Anti-Localization Effect in Topological Insulator Bi_2Se_3. *Phys. Rev. B* **84**, 073109 (2011).
15. Liu, M. *et al.* Crossover Between Weak Antilocalization and Weak Localization in a Magnetically Doped Topological Insulator. *Phys. Rev. Lett.* **108**, 036805 (2012).
16. Cao, H. L. *et al.* Quantized Hall Effect and Shubnikov – de Haas Oscillations in Highly Doped Bi_2Se_3: Evidence for Layered Transport of Bulk Carriers. *Phys. Rev. Lett.* **108**, 216803 (2012).
17. He, H. T. *et al.* Impurity Effect on Weak Antilocalization in the Topological Insulator Bi_2Te_3. *Phys. Rev. Lett.* **106**, 166805 (2011).
18. Steinberg, H., Gardner, D. R., Lee, Y. S. & Jarillo-Herrero, P. Surface State Transport and Ambipolar Electric Field Effect in Bi_2Se_3 Nanodevices. *Nano Lett.* **10**, 5032–5036 (2010).
19. Ren, Z., Taskin, A. A., Sasaki, S., Segawa, K. & Ando, Y. Large Bulk Resistivity and Surface Quantum Oscillations in the Topological Insulator Bi_2Te_2Se. *Phys. Rev. B* **82**, 241306(R) (2010).
20. Taskin, A. A., Ren, Z., Sasaki, S., Segawa, K. & Ando, Y. Observation of Dirac Holes and Electrons in a Topological Insulator. *Phys. Rev. Lett.* **107**, 016801 (2011).
21. Kim, D. *et al.* Surface Conduction of Topological Dirac Electrons in Bulk Insulating Bi_2Se_3. *Nat. Phys.* **8**, 459–463 (2012).
22. Tang, H., Liang, D., Qiu, L. J. & Gao, P. A. X. Two-Dimensional Transport-Induced Linear Magneto-Resistance in Topological Insulator Bi_2Se_3 Nanoribbons. *ACS Nano* **5**, 7510–7516 (2011).
23. Tian, M. *et al.* Dual Evidence of Surface Dirac States in Thin Cylindrical Topological Insulator Bi_2Te_3 Nanowires. *Sci. Rep.* **3**, 1212 (2013).
24. Edmonds, M. T. *et al.* Air-Stable Electron Depletion of Bi_2Se_3 Using Molybdenum Trioxide into the Topological Regime. *ACS Nano* **8**, 6400–6406 (2014).
25. Sacepe, B. *et al.* Gate-Tuned Normal and Superconducting Transport at the Surface of a Topological Insulator. *Nat. Commun.* **2**, 575 (2011).
26. Kozlov, D. A. *et al.* Transport Properties of a 3D Topological Insulator Based on a Strained High Mobility HgTe Film. *Phys. Rev. Lett.* **112**, 196801 (2014).
27. Fu, Y. S. *et al.* Memory Effect in a Topological Surface State of Bi_2Te_2Se. *ACS Nano* **7**, 4105–4110 (2013).
28. Xia, B. *et al.* Indication of Surface – Dominated Transport in Single Crystalline Nanoflake Devices of Topological Insulator $Bi_{1.5}Sb_{0.5}Te_{1.8}Se_{1.2}$. *Phys. Rev. B* **87**, 085442 (2013).
29. Bao, L. *et al.* Weak Anti-Localization and Quantum Oscillations of Surface States in Topological Insulator Bi_2Se_2Te. *Sci. Rep.* **2**, 276 (2012).
30. Xu, R. *et al.* Large Magnetoresistance in Non-Magnetic Silver Chalcogenides. *Nature* **390**, 57–60 (1997).
31. Husmann, A. *et al.* Megagauss Sensors. *Nature* **417**, 421–424 (2002).
32. Parish, M. M. & Littlewood, P. B. Non-saturating Magnetoresistance in Heavily Disordered Semiconductors. *Nature* **426**, 162–165 (2003).
33. Zhang, W. *et al.* Topological Aspect and Quantum Magnetoresistance of β-Ag_2Te. *Phys. Rev. Lett.* **106**, 156808 (2011).
34. Sulaev, A. *et al.* Experimental Evidences of Topological Surface States of β-Ag_2Te. *AIP Adv.* **3**, 032123 (2013).
35. Lee, S. G. *et al.* Single Crystalline β-Ag_2Te Nanowires as a New Topological Insulator. *Nano Lett.* **12**, 4194–4199 (2012).
36. Fritzsche, H. Electrical Properties of Germanium Semiconductors at Low Temperatures. *Phys. Rev.* **99**, 406 (1955).
37. Lang, M. *et al.* Revelation of Topological Surface States in Bi_2Se_3 Thin Films by *In Situ* Al Passivation. *ACS Nano* **6**, 295–302 (2011).
38. Shoenberg, D. *Magnetic Oscillations in Metals* (Cambridge University Press, 1984).
39. Hamdou, B., Gooth, J., Dorn, A., Pippel, E. & Nielsch, K. Surface State Dominated Transport in Topological Insulator Bi_2Te_3 Nanowires. *Appl. Phys. Lett.* **103**, 193107 (2013).
40. Gehring, P., Gao Bo, F., Burghard, M. & Kern, K. Growth of High-Mobility Bi_2Te_2Se Nanoplatelets on hBN Sheets by van der Waals Epitaxy. *Nano Lett.* **12**, 5137–5142 (2012).
41. Reinthaler, R. W. & Hankiewicz, E. M. Interplay of Bulk and Edge States in Transport of Two-Dimensional Topological Insulators. *Phys. Rev. B* **85**, 165450 (2012).

Acknowledgments

We thank Ming Liang Tian for helpful discussions. This work was supported by the Ministry of Education of Singapore (Grant NO: MOE2010-T2-2-059), the Singapore A*STAR SERC 102 101 0019, and the National Science Foundation of China, Grant No. 61376127.

Author contributions

W.L. conceived the idea and supervised the research. A.S. and W.L. designed and performed the experiments. A.S. and Z.W.G fabricated the devices. A.S. and W.L. carried out low-temperature transport measurements. A.S., K.L.T. and W.L. contributed to the analysis. A.S. and W.L. wrote the paper with helps of all other co-authors.

Additional information

Competing financial interests: The authors declare no competing financial interests.

How to cite this article: Sulaev, A., Zhu, W., Teo, K.L. & Wang, L. Gate-tuned quantum oscillations of topological surface states in β-Ag_2Te. *Sci. Rep.* **5**, 8062; DOI:10.1038/srep08062 (2015).